Near-infrared Faraday rotation of $Cd_{1-x}Mn_xTe$

H. J. Jiménez-González and R. L. Aggarwal*
Francis Bitter National Magnet Laboratory, Massachusetts Institute of Technology, Cambridge, Massachusetts 02139 and Department of Physics, Massachusetts Institute of Technology, Cambridge, Massachusetts 02139

P. Becla
Francis Bitter National Magnet Laboratory, Massachusetts Institute of Technology, Cambridge, Massachusetts 02139
(Received 8 January 1992)

The near-infrared Faraday rotation of $Cd_{1-x}Mn_xTe$ has been measured for $x = 0$–0.3 at 300 and 77 K for photon energies between 0.1 (12.0) and 1.5 (0.8) eV (μm). We have developed a multioscillator model for the Faraday rotation using an analytical expression for the refractive index that includes contributions from interband transitions at the Γ, L, and X points of the Brillouin zone, as well as the lattice contribution from optical phonons. The multioscillator model explains the measured behavior of the Verdet constant as a function of photon energy for all concentrations at both temperatures. This model has also been applied successfully to Faraday rotation data for $Cd_{1-x}Mn_xTe$ and $Zn_{1-x}Mn_xTe$ from previous studies.

I. INTRODUCTION

Diluted magnetic semiconductors (DMS's) are known to have a large Faraday rotation at photon energies near the band gap. This is the result of an enhanced Zeeman splitting of the band electrons caused by the *sp-d* exchange interaction between the magnetic moments of transition-metal ions, such as Mn^{2+}, and the free-carrier spins.[1] The present work was motivated by the possibility of using DMS's as infrared Faraday isolators at room temperature, particularly in the 10-μm region of the CO_2 laser. In 1983 Turner, Gunshor, and Datta[2] reported room-temperature measurements of the $Cd_{0.55}Mn_{0.45}Te$ Faraday rotation for wavelengths up to 1.0 μm (1.2 eV). More recently, Bartholomew, Furdyna, and Ramdas[3] and Nikitin and Savchuk[4] reported more detailed studies of Faraday rotation in $Cd_{1-x}Mn_xTe$ and $Zn_{1-x}Mn_xTe$ in the same wavelength region. Our work explores the spectral region between 0.825 (1.5) and 12.0 (0.1) μm (eV) at 300 and 77 K for Mn concentration $x = 0$, 0.05, 0.08, 0.18, and 0.27.

Bartholomew, Furdyna, and Ramdas,[3] Nikitin and Savchuk,[4] and Butler,[5] among others, have analyzed their Faraday rotation data for $Cd_{1-x}Mn_xTe$ and $Zn_{1-x}Mn_xTe$ in terms of a single-oscillator model for the index of refraction involving an interband excitonic transition at the fundamental gap $\mathcal{E}_0$. Although this model yields good results for Mn concentrations $x \gtrsim 0.05$, at lower values of x it is unable to account for the observed change in the sign of the Verdet constant of $Cd_{1-x}Mn_xTe$ and $Zn_{1-x}Mn_xTe$ as a function of photon energy.[3] We believe that the success of their single-oscillator model is fortuitous, to some extent, since at 300 and 77 K their model does not adequately describe the index of refraction of $Cd_{1-x}Mn_xTe$ or $Zn_{1-x}Mn_xTe$. Pikhtin and Yas'kov[6] fitted the measured refractive index n of various semiconductors, with diamond and zinc-blende structures, to a multioscillator model that includes contributions from interband transitions at the L and X points in the Brillouin zone in addition to the fundamental-gap contribution at the Γ point. We have used this analytical form of n to derive an expression for Θ_F. We interpret our Faraday rotation data in terms of transitions at the Γ and L points in the Brillouin zone. The higher-energy transitions at the L point are found to be responsible for the sign reversal of the Verdet constant as a function of photon energy. This effect has been observed at small x for both $Cd_{1-x}Mn_xTe$ and $Zn_{1-x}Mn_xTe$ (see Bartholomew, Furdyna, and Ramdas[3]).

II. THEORETICAL BACKGROUND

For the model describing Faraday rotation we consider linearly polarized light propagating through a material of length L in the direction of $\mathbf{B}$. After traveling through the material, the electric-field polarization vector $\mathbf{E}$ makes an angle Θ_F with the initial polarization direction.

Faraday rotation results from the difference in phase velocity of left (σ^-) and right (σ^+) circularly polarized light propagating through a medium along $\mathbf{B}$. (Right and left circularly polarized light are defined as having positive and negative helicity with respect to time, respectively.) The phase difference $\Delta\varphi$ between the two circularly polarized components after propagation through a distance L is given by

$$\Delta\varphi = \frac{\omega L}{c}(n_- - n_+) \tag{1}$$

in the cgs system; ω is the angular frequency of the light, c is the speed of light in vacuum, and n_- and n_+ are the indices of refraction for σ^- and σ^+ polarizations, re-

spectively. The Faraday rotation angle Θ_F is then given by

$$\Theta_F = \tfrac{1}{2}\Delta\varphi = \frac{\omega L}{2c}(n_- - n_+) = \frac{\mathcal{E}L}{2\hbar c}(n_- - n_+), \quad (2)$$

where $\mathcal{E}$ is the photon energy $\hbar\omega$ and $\hbar$ is Planck's constant divided by 2π. For undoped wide-gap semiconductors, only conduction to valence interband contributions are significant.

To calculate the zero-field refractive index n we used the multioscillator model derived by Pikhtin and Yas'kov,[6]

$$n^2 = 1 + \frac{0.7}{\pi\sqrt{\mathcal{E}_0}} \ln\frac{\mathcal{E}_1^2 - \mathcal{E}^2}{\mathcal{E}_0^2 - \mathcal{E}^2} + \frac{G_1}{\mathcal{E}_1^2 - \mathcal{E}^2} + \frac{G_2}{\mathcal{E}_2^2 - \mathcal{E}^2} + \frac{G_{\rm TO}}{\mathcal{E}_{\rm TO}^2 - \mathcal{E}^2}, \quad (3)$$

where $\mathcal{E}_0$, $\mathcal{E}_1$, and $\mathcal{E}_2$ are the band gaps at or near the Γ, L, and X points in the Brillouin zone, respectively, and $\mathcal{E}_{\rm TO}$ is the energy of the zone-center TO phonons. G_1, G_2, and $G_{\rm TO}$ are the corresponding oscillator strengths for the $\mathcal{E}_1$, $\mathcal{E}_2$, and $\mathcal{E}_{\rm TO}$ transitions.

This expression for n is obtained from the application of the Kramers-Kronig relations to the imaginary part of the dielectric constant $\epsilon_2(\omega)$ in the limit of low absorption. For photon energies lower than $\mathcal{E}_0$ the details of the $\epsilon_2(\omega)$ dispersion are not important and we need to keep only the major features.[6] It is possible then to model $\epsilon_2(\omega)$ as a constant between $\mathcal{E}_0$ and $\mathcal{E}_1$ followed by two undamped oscillators at $\mathcal{E}_1$ and $\mathcal{E}_2$ as shown in Fig. 1. Between $\mathcal{E}_0$ and $\mathcal{E}_1$ we take a constant amplitude A of $0.7\mathcal{E}_0^{-1/2}$ which is the average of $\epsilon_2(\omega)$.[6] In contrast to the single-oscillator model, the multioscillator model *does not assume that the fundamental absorption is due to an exciton with oscillator strength concentrated at* $\mathcal{E}_0$. The absorption edge is modeled as a step function. This is a reasonable approximation for transitions that are nonexcitonic or weakly excitonic in nature.

The measured index of refraction[7] was fitted to Eq. (3) to obtain G_1 and G_2 using measured energy gaps.[8] Using the Lyddane-Sachs-Teller relation and Eq. (3), $G_{\rm TO}$ can be related to the other constants and the energy of the LO phonon $\mathcal{E}_{\rm LO}$ through[6]

$$G_{\rm TO} = \left(1 + \frac{0.7}{\pi\sqrt{\mathcal{E}_0}} \ln\frac{\mathcal{E}_1^2}{\mathcal{E}_0^2} + \frac{G_1}{\mathcal{E}_1^2} + \frac{G_2}{\mathcal{E}_2^2}\right)(\mathcal{E}_{\rm LO}^2 - \mathcal{E}_{\rm TO}^2). \quad (4)$$

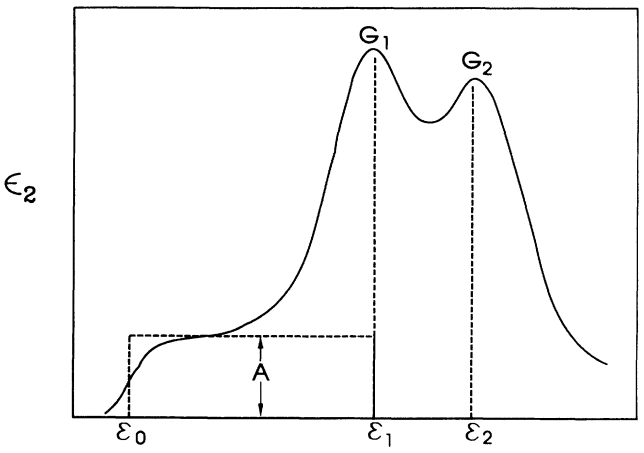

FIG. 1. Schematic spectrum of the imaginary part of the dielectric constant ϵ_2 for a typical zinc-blende semiconductor. The model used to approximate ϵ_2 is shown as a dashed line.

Values for these constants are shown in Table I.

Figure 2 shows the best fit to the room-temperature refractive index of CdTe (Ref. 7) using the single-oscillator model and the multioscillator model of Pikhtin and Yas'kov.[6] In the single-oscillator model, n is given by

$$n^2 = n_0^2 + \frac{F_0}{\mathcal{E}_0^2 - \mathcal{E}^2}, \quad (5)$$

where n_0 and F_0 are used as fitting parameters. Bartholomew, Furdyna, and Ramdas[3] and Nikitin and Savchuk[4] have used an approximation in which n_0^2 is dropped compared to the second term of Eq. (5). Such an approximation leads to a Verdet constant $\propto \mathcal{E}^2(\mathcal{E}_0^2 - \mathcal{E}^2)^{-3/2}$. From the best fit to the room-temperature CdTe data we obtain $n_0^2 = 7.2$ and $F_0 = 0.15$ eV^2. Using $\mathcal{E}_0 = 1.528$ eV (Ref. 8) we note that, even for $\mathcal{E} = 1.500$ eV, dropping n_0^2 in Eq. (5) is not a good approximation. Without this approximation the Verdet constant would be $\propto \mathcal{E}^2(\mathcal{E}_0^2 - \mathcal{E}^2)^{-2}$, since n_0^2 is the dominant term in Eq. (5) for most energies.

For small $\Delta\mathcal{E}_i$ the difference $(n_- - n_+)$ can be expressed as

$$(n_- - n_+) \simeq \sum_i \frac{\partial n}{\partial \mathcal{E}_i}\Delta\mathcal{E}_i, \quad (6)$$

TABLE I. Dispersion parameters for the index of refraction of CdTe and ZnTe.

Material	E_0 (eV)[a]	E_1 (eV)[b]	E_2 (eV)[b]	$E_{\rm TO}$ (meV)[c]	$E_{\rm LO}$ (meV)	G_1 (eV^2)	G_2 (eV^2)
CdTe (300 K)	1.528	3.50	5.50	17.40	20.80[e]	66.467	12.74
CdTe (77 K)	1.613[d]	3.62	5.59	18.23	21.08[e]	46.556	71.26
ZnTe (33 K)	2.271	3.70	5.50	23.60	25.78[f]	34.289	109.17

[a]Reference 8.
[b]References 9 and 10.
[c]References 11 and 12.
[d]Reference 6.
[e]Reference 13.
[f]Reference 6.

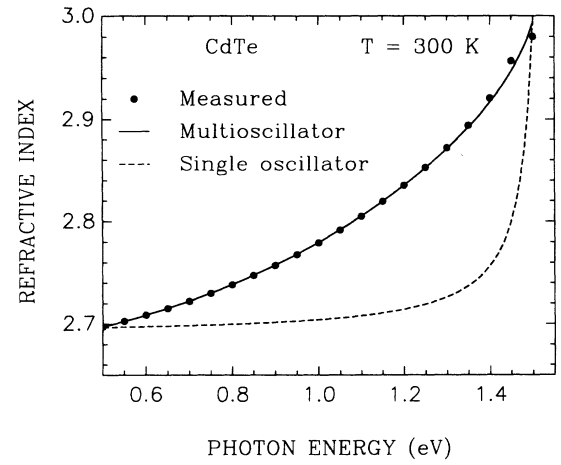

FIG. 2. Best fit to the room-temperature refractive index of CdTe, using the single-oscillator and multioscillator models described in the text.

where the index i runs over the various transitions contributing to n and $\Delta\mathcal{E}_i = \mathcal{E}_- - \mathcal{E}_+$ is the difference between the transition energies for the σ^- and σ^+ polarizations in the presence of a magnetic field. For $\mathcal{E} < \mathcal{E}_0$ we evaluate the sum in Eq. (6) for $\mathcal{E}_0$ and $\mathcal{E}_1$ and ignore contributions for $\mathcal{E}_2$ and $\mathcal{E}_{TO}$. This is a reasonable approximation since, for the wavelengths of interest, the dispersion from $\mathcal{E}_2$ and $\mathcal{E}_{TO}$ is relatively small (see dispersion parameters in Table I). Using Eq. (3) we obtain

$$\frac{\partial n}{\partial \mathcal{E}_i} = \frac{1}{2n}\frac{\partial n^2}{\partial n_i}. \tag{7}$$

Taking partial derivatives with respect to $\mathcal{E}_0$ and $\mathcal{E}_1$ we get

$$\frac{\partial n}{\partial \mathcal{E}_0} = -\frac{0.7}{n\pi\mathcal{E}_0^{\frac{3}{2}}}\left[\tfrac{1}{4}\ln\left(\frac{\mathcal{E}_1^2-\mathcal{E}^2}{\mathcal{E}_0^2-\mathcal{E}^2}\right)+\frac{\mathcal{E}_0^2}{\mathcal{E}_0^2-\mathcal{E}^2}\right], \tag{8a}$$

$$\frac{\partial n}{\partial \mathcal{E}_1} = -\frac{\mathcal{E}_1}{n(\mathcal{E}_1^2-\mathcal{E}^2)^2}\left[G_1 - \frac{0.7}{\pi\sqrt{\mathcal{E}_0}}(\mathcal{E}_1^2-\mathcal{E}^2)\right]. \tag{8b}$$

Using Eqs. (2), (6), (8a), and (8b) we obtain

$$\Theta_F = -\frac{\mathcal{E}L}{2\hbar c}\left[\frac{\partial n}{\partial \mathcal{E}_0}\Delta\mathcal{E}_0 + \frac{\partial n}{\partial \mathcal{E}_1}\Delta\mathcal{E}_1\right]. \tag{9}$$

We consider two contributions to the magnetic-field-induced energy splitting at the Γ point: (i) the conventional Zeeman splitting (as observed in CdTe) and (ii) the exchange-induced splitting. We can express $\Delta\mathcal{E}_0$ as $\Delta\mathcal{E}_0^{(Z)} + \Delta\mathcal{E}_0^{(E)}$ where the superscripts (Z) and (E) represent Zeeman and exchange interactions, respectively. $\Delta\mathcal{E}_0^{(Z)}$ is determined from experiment and $\Delta\mathcal{E}_0^{(E)}$ can be expressed as[3]

$$\Delta\mathcal{E}_0^{(E)} = \frac{(\alpha-\beta)}{g_{Mn}\mu_B}M, \tag{10}$$

where α and β are exchange constants for the conduction- and valence-band electrons, respectively, $g_{Mn} = 2$ is the Landé g factor of the Mn^{2+} ions, μ_B is the Bohr magneton, and M is the magnetization. At high temperatures the magnetization is given by[14]

$$M = \chi B = \frac{C(x)}{T-\Theta(x)}B, \tag{11}$$

where

$$C(x) = \frac{xN_0(g_{Mn}\mu_B)^2S(S+1)}{3k_B},$$

and $\Theta(x) = \Theta_0 x$ with $\Theta_0 < 0$. This approximation is valid for $\Theta(x) \ll T$. Using this we obtain

$$M = \frac{xN_0(g_{Mn}\mu_B)^2S(S+1)}{3k_BT(1-\frac{\Theta_0}{T}x)}B, \tag{12}$$

where N_0 is the number of Mn^{2+} ions per unit volume, $S = \frac{5}{2}$ is the spin of the Mn^{2+} ions, k_B is the Boltzmann constant, and Θ_0 is a constant of the material having values of -470 and -831 for $Cd_{1-x}Mn_xTe$ and $Zn_{1-x}Mn_xTe$, respectively.[14] Combining expressions for $\Delta\mathcal{E}_0^{(E)}$ and $\Delta\mathcal{E}_0^{(Z)}$, we obtain

$$\Delta\mathcal{E}_0 = \left[\frac{xN_0(\alpha-\beta)g_{Mn}\mu_BS(S+1)}{3k_BT(1-\frac{\Theta_0}{T}x)} + \Delta\mathcal{E}_0^{(Z)}\right]B, \tag{13}$$

where $N_0(\alpha-\beta) = 1.10$ eV and $\Delta\mathcal{E}_0^{(Z)} = -8.0\times10^{-6}$ eV/kG for $Cd_{1-x}Mn_xTe$ (Refs. 15 and 16) and $N_0(\alpha-\beta) = 1.28$ eV for $Zn_{1-x}Mn_xTe$.[17,18] The value of $\Delta\mathcal{E}_0^{(Z)}$ for $Zn_{1-x}Mn_xTe$ is determined from the data analysis (see Sec. IV). The exchange splitting of $Cd_{1-x}Mn_xTe$ at the L point has been measured by Ginter, Gaj, and Si Dang.[19] The magnitude of the splitting is approximately 26 times smaller than that at the Γ point and it has the same sign. The Zeeman contribution at the L point is expressed as

$$\Delta\mathcal{E}_1^{(Z)} = g_1^*\mu_BB, \tag{14}$$

where g_1^* is an effective interband g factor at the L point, used here as a fitting parameter. Thus for $Cd_{1-x}Mn_xTe$,

$$\Delta\mathcal{E}_1 = \left[\frac{1}{26}\frac{xN_0(\alpha-\beta)g_{Mn}\mu_BS(S+1)}{3k_BT(1-\frac{\Theta_0}{T}x)} + g_1^*\mu_B\right]B. \tag{15}$$

Since we have no information about the L-point exchange splitting for $Zn_{1-x}Mn_xTe$, the total-energy splitting is approximated as

$$\Delta\mathcal{E}_1 = \gamma\mu_BB, \tag{16}$$

where γ is a fitting parameter. The total interband Faraday rotation is then obtained by inserting Eqs. (8a), (8b), (13), (15), and (16) into Eq. (9).

At $T = 77$ K we adopt a phenomenological form of M given by[3]

$$M = \frac{C(x)}{T+T_{AF}}B,$$

where T_{AF} is used as a fitting parameter. We find that for

$x = 0.047$, the value obtained for T_{AF} is close to $470x$ as in the high-temperature approximation of Eq. (11). For $x = 0.076$, however, the value of T_{AF} deviates significantly from $470x$.

We obtained the 77-K refractive index of CdTe from the temperature-dependent Sellmeier coefficients generated by Barnes and Piltch[20] using the data of Harvey and Wolfe.[21]

III. EXPERIMENTAL PROCEDURE

Single crystals of $Cd_{1-x}Mn_xTe$ were grown using the Bridgman method. The Mn concentration of the four samples used was determined from atomic absorption by Northern Analytical Laboratory[22] at $(4.7 \pm 0.2)\%$, $(7.6 \pm 0.4)\%$, $(17.9 \pm 0.94)\%$, and $(26.8 \pm 1.3)\%$. The samples were cut and polished, then etched in a 5% solution of bromine in methanol for approximately 1 min. The samples are p type with carrier concentrations of $\sim 10^{14}$ cm^{-3}. Samples with 7.6% and 26.8% Mn were used as grown, while the 4.7% and 17.9% samples were annealed in a Cd-rich atmosphere at 800 °C for 5 days.

Faraday rotation measurements at $T = 77$ K were made using a cryostat with a KBr room-temperature window and a ZnSe cold window. A 2-in. bore Bitter magnet provided dc magnetic fields of up to 150 kG. A tungsten halogen lamp and an air-cooled coilform were the radiation sources for $\lambda < 1.0$ and $\lambda > 1.0$ μm, respectively. The linear polarizers used were Polaroid HR,[23] for $\lambda < 2.0$ μm, and PTR Optics[24] wiregrid for $\lambda > 2.0$ μm. We used a 0.22-m Spex[25] model 1680B double-grating monochromator. The detector was a liquid-helium-cooled Ge bolometer from Infrared Laboratories.[26] Details of the experimental determination of Θ_F are provided in the Appendix.

IV. RESULTS AND DISCUSSION

Figures 3 and 4 show the room-temperature Verdet constant for $Cd_{1-x}Mn_xTe$ as a function of photon energy. The data were fitted to the multioscillator model using Eq. (9). The only fitting parameters used were g_1^* and $\mathcal{E}_0$.

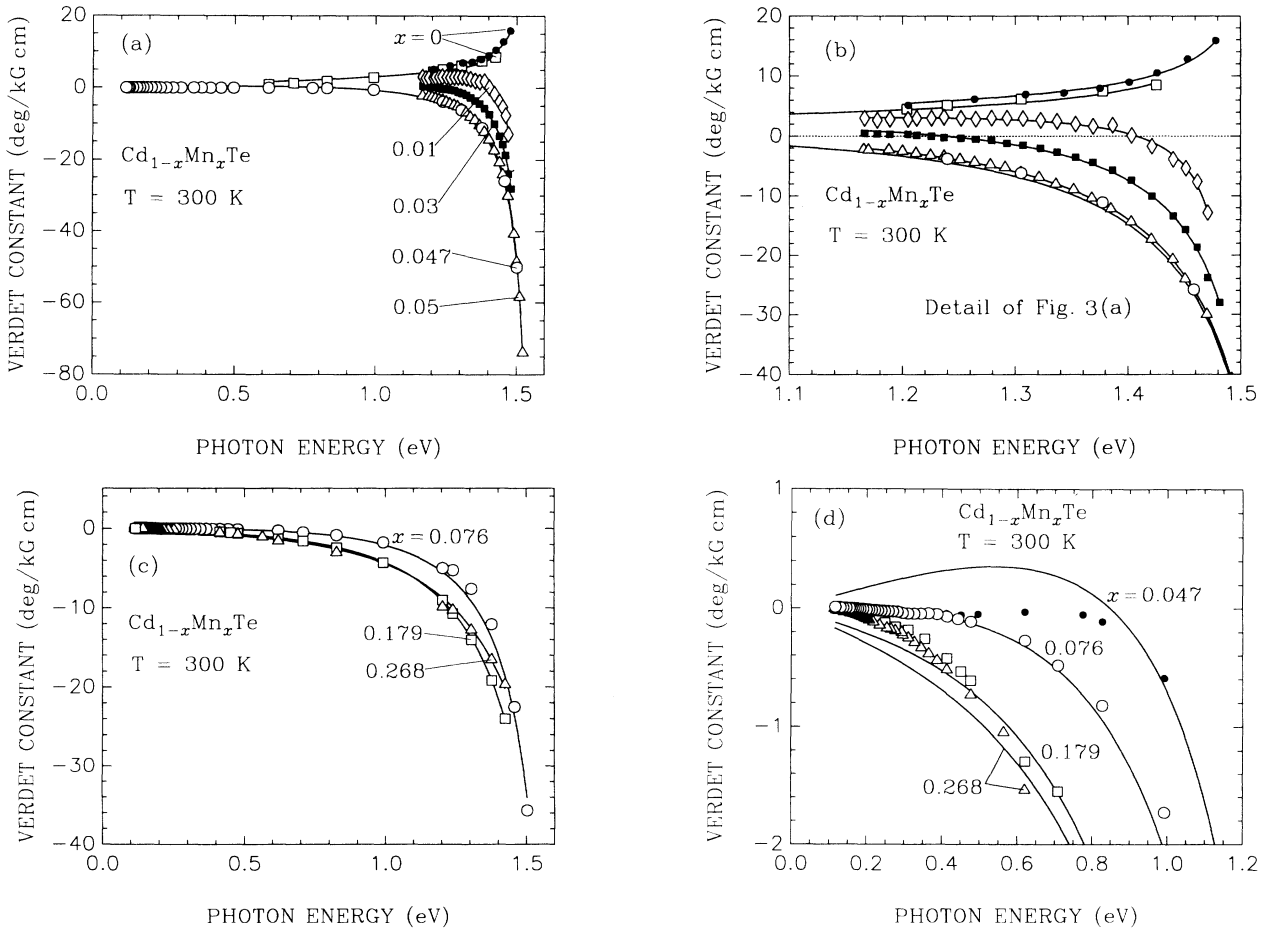

FIG. 3. Room-temperature Faraday rotation of $Cd_{1-x}Mn_xTe$ for various Mn concentrations as a function of photon energy. Solid lines indicate the best fit to the multioscillator model. Some data by other authors have been included: in (a) solid circles are from Ref. 4, open diamonds, closed squares, and open triangles are from Ref. 3. (b) is a detail of (a) in the region of zero crossing. (c) shows the Verdet constant for $x = 0.076$, 0.179, and 0.268. (d) shows the long-wavelength data in an expanded scale.

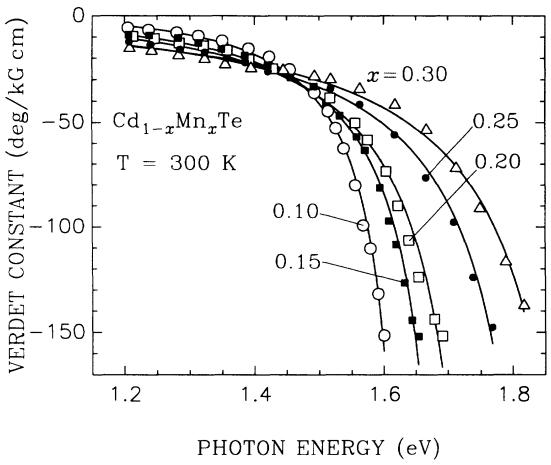

FIG. 4. Room-temperature Faraday rotation of $Cd_{1-x}Mn_xTe$ for various Mn concentrations as a function of photon energy, measured by Nikitin and Savchuk (Ref. 4). Solid lines indicate the best fit to the multioscillator model.

Figure 3(a) shows the Verdet constant for low values of x. This figure includes data from Bartholomew, Furdyna, and Ramdas.[3] Figure 3(b) is a detail of Fig. 3(a), which shows the change in the sign of V as x increases from 0% to 5%. In Fig. 3(c) we show the Verdet constant for $x > 0.05$. Figure 3(d) shows the long-wavelength Faraday rotation for $Cd_{1-x}Mn_xTe$. The agreement between the data and the multioscillator model in this wavelength region is not as good as in the shorter-wavelength region; this may be due to the neglect of small contributions from impurities and other defects. Figure 4 shows data of Nikitin and Savchuk[4] fitted to the multioscillator model. We observe that beyond $\sim$ 1.5 eV the ordering of the curves is reversed since the band-gap resonance occurs at lower energies for small x. A similar crossing can also be seen in Fig. 3(c). As shown in Table II, the values for $\mathcal{E}_0$ obtained from the fitting are reasonably close to the measured values.

Figure 5 shows a similar set of curves for $Zn_{1-x}Mn_xTe$. The zero-crossing occurs at a higher value of x than for $Cd_{1-x}Mn_xTe$, indicating that $Zn_{1-x}Mn_xTe$ has a larger ratio of $\Delta\mathcal{E}_1/\Delta\mathcal{E}_0$ than $Cd_{1-x}Mn_xTe$. Fitting parameters for $Zn_{1-x}Mn_xTe$ are also found in Table II. Figure 6 shows g_1^* and γ as a function of x for $Cd_{1-x}Mn_xTe$ and $Zn_{1-x}Mn_xTe$, respectively, at 300 K. In both materials g_1^* (γ) has the same sign as the conduction-band g factor at the Γ point and increases monotonically with Mn concentration. Note that for $Zn_{1-x}Mn_xTe$, the parameter γ includes both the Zeeman and exchange contributions.

We can see from Figs. 3(b) and 5 that the model can successfully describe the zero-crossing of the Verdet constant observed at low Mn concentrations. The contribution to the Faraday rotation due to the gap at the L point is responsible for the change of sign of the Verdet constant. In $Cd_{1-x}Mn_xTe$, the Zeeman contribution to $\Delta\mathcal{E}_1$ is larger than the exchange contribution for most concentrations, while at the Γ point the exchange contribution

TABLE II. Fitting parameters for the Faraday rotation of $Cd_{1-x}Mn_xTe$ and $Zn_{1-x}Mn_xTe$.

Material	x (%)	Reference	E_0 (eV)[d]	E_0^{fit} (eV)	$-g_1^*$ ($-\gamma$)[e]
$Cd_{1-x}Mn_xTe$ (300 K)	0	a	1.528	1.530	0.4
	0	c	1.528	1.530	0.5
	1	b	1.541	1.500	0.9
	3	b	1.567	1.542	1.4
	4.7	a	1.589	1.570	1.7
	5	b	1.594	1.570	1.8
	7.6	a	1.627	1.646	2.2
	10	c	1.660	1.650	3.5
	15	c	1.725	1.721	3.7
	17.9	a	1.762	1.747	4.2
	20	c	1.791	1.780	4.8
	25	c	1.857	1.876	4.1
	26.8	a	1.879	1.859	5.2
	30	c	1.923	1.950	4.3
$Cd_{1-x}Mn_xTe$ (77 K)	4.7	a	1.656	1.656	5.6
	7.6	a	1.700	1.700	10.6
$Zn_{1-x}Mn_xTe$ (300 K)	0	b	2.271	2.310	0.6
	2	b	2.281	2.260	1.2
	5	b	2.297	2.300	2.0
	10	b	2.323	2.320	2.8

[a]This paper.
[b]Reference 3.
[c]Reference 4.
[d]References 8 and 27.
[e]γ applies to $Zn_{1-x}Mn_xTe$.

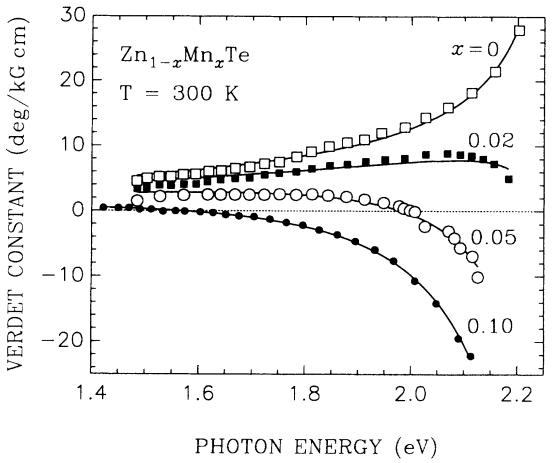

FIG. 5. Room-temperature Faraday rotation of $Zn_{1-x}Mn_xTe$ for various Mn concentrations as a function of photon energy, measured by Bartholomew, Furdyna, and Ramdas (Ref. 3). Solid lines indicate the best fit to the multioscillator model.

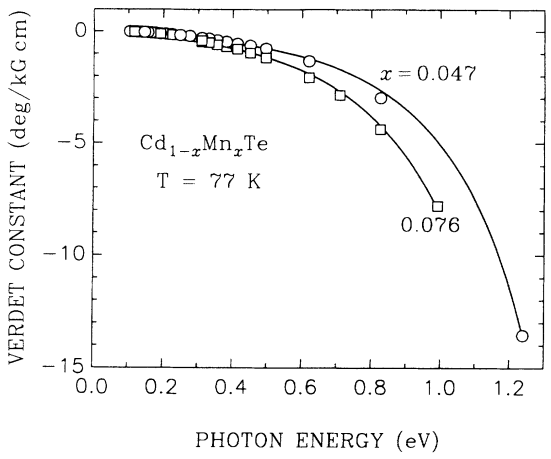

FIG. 7. Faraday rotation of $Cd_{1-x}Mn_xTe$ at 77 K for $x = 0.047$ and 0.076. Solid lines represent the best fit to the multioscillator model.

dominates for $x \gtrsim 0.005$. This results in $\Delta\mathcal{E}_0$ and $\Delta\mathcal{E}_1$ having opposite signs. Furthermore, the L-point contribution to Θ_F is dominant at low energies and low Mn concentrations, thus accounting for the zero crossing in the data.

To fit the room-temperature $Zn_{1-x}Mn_xTe$ data, we first used $\Delta\mathcal{E}_0^{(Z)}$ as a fitting parameter at $x = 0$. This procedure yields $\Delta\mathcal{E}_0^{(Z)} = -3.0\times10^{-5}$ eV/kG. This value is then used to fit the data for $x \neq 0$. $\Delta\mathcal{E}_1$ was modeled as $\gamma\mu_B B$ because of the lack of information about the L-point exchange splitting in this material.

Figure 7 shows the Faraday rotation of $Cd_{1-x}Mn_xTe$ at 77 K for $x = 0.047$ and 0.076. In fitting the 77-K data we assumed that the ratio $\Delta\mathcal{E}_0^{(E)}/\Delta\mathcal{E}_1^{(E)}$ is the same as that for 300 K. The values of $\mathcal{E}_1$ and $\mathcal{E}_2$ were adjusted using $d\mathcal{E}_1/dT = -5.5\times10^{-4}$ eV/K and $d\mathcal{E}_2/dT = -4.1\times10^{-4}$ eV/K.[28] Values of the fitting parameters are given in Table II. For the T_{AF} parameter we obtained values of 36.9 and 19.8 K for $x = 0.047$ and 0.076, respectively.

The success of the model at both 300 and 77 K indicates that excitonic effects at the absorption edge are not sufficiently strong to justify the use of a single-oscillator approximation at these temperatures. It is remarkable that the predicted $\mathcal{E}_0$'s are close to the measured ones, considering that the behavior of ϵ_2 at the Γ point has been crudely modeled as a constant for both temperatures.

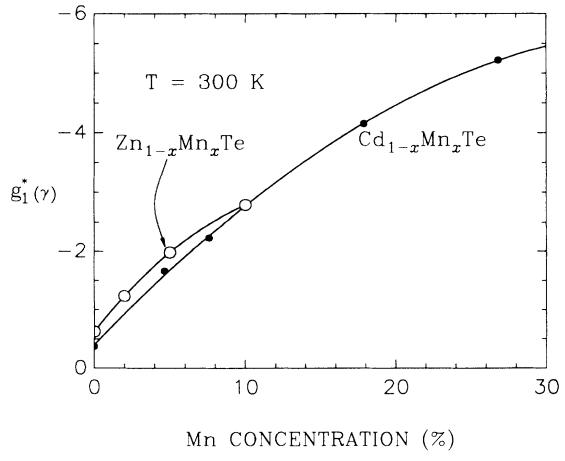

FIG. 6. Room-temperature effective interband g factor at the L point, $g_1^*(\gamma)$, as a function of Mn concentration for $Cd_{1-x}Mn_xTe$ and $Zn_{1-x}Mn_xTe$.

ACKNOWLEDGMENTS

We express our gratitude to G. Favrot and Dr. O. W. Shih for their valuable suggestions and discussions and Dr. D. Heiman for a critical reading of the manuscript. This work is supported in part by Lincoln Laboratory. The Francis Bitter National Magnet Laboratory is supported by NSF Cooperative Agreement DMR-8813164.

APPENDIX: ANALYSIS OF FARADAY ROTATION MEASUREMENTS

In the following we summarize the mathematical framework for the interpretation of Faraday rotation measurements. Our measurements cover such a wide range of wavelengths that in some cases the polarizers become imperfect and can transmit some light with the undesired polarization. The following analysis takes into account this possibility. It also makes corrections for multiple reflections at the faces of the sample so that the rotation angle extracted from the measurement corresponds to a single pass through the material.

A beam of light that is initially polarized along the $\hat{x}$ direction can be expressed in terms of its left (ℓ) and right (r) circularly polarized components as they traverse the medium along the z direction as

$$\mathbf{E} = \tfrac{1}{2}E_0(\epsilon_1\hat{x} + \epsilon_2\hat{y}), \tag{A1}$$

where

$$\epsilon_1 = \left[e^{ik_r z}e^{-\alpha_r z/2} + e^{ik_l z}e^{-\alpha_l z/2}\right],$$
$$\epsilon_2 = i\left[e^{ik_r z}e^{-\alpha_r z/2} - e^{ik_l z}e^{-\alpha_l z/2}\right], \tag{A2}$$

E_0 is a constant amplitude, k is the propagation constant, α is the absorption coefficient, and z is the coordinate along the propagation direction.

When the initial polarizer is oriented along $\hat{x}$, a small fraction s of the electric field along $\hat{y}$ will also get through. After some algebra, we obtain an expression for the transmitted intensity,[29]

$$I_{N(R)} = \tfrac{1}{4}E_0^2(1-R)^2(1+s^2)\left\{\left[\frac{e^{-\alpha_r z}}{1-R^2e^{-2\alpha_r z}} + \frac{e^{-\alpha_l z}}{1-R^2e^{-2\alpha_l z}}\right]\right.$$
$$+\frac{2\gamma e^{-(\alpha_r+\alpha_l)z/2}[1-R^2e^{-2(\alpha_r+\alpha_l)z}]}{1-2R^2e^{-(\alpha_r+\alpha_l)z}\cos 2(k_r-k_l)z + R^4e^{-2(\alpha_r+\alpha_l)z}}$$
$$\left.\times\left[\cos 2\varphi\cos(k_r-k_l)z \mp \beta\sin 2\varphi\sin(k_r-k_l)z\right]\right\}, \tag{A3}$$

where the subscripts N and R refer to the magnetic field in the normal and reverse directions, respectively, R is the surface reflectivity, γ measures the leakage perpendicular to the transmission axis of the analyzer and polarizer, and φ is the angle between $\hat{x}$ and the transmission axis of the analyzer. The magnetic-field reversal results in the exchange of the (r, ℓ) labels in the above equations. In the limit where $\alpha = 0$ and $\varphi = \frac{\pi}{4}$,

$$\sin 2\Theta_F = \frac{\Delta I}{\beta\gamma}\left(1 + \eta\sin^2 2\Theta_F\right), \tag{A4}$$

where

$$\Delta I = \frac{I_R - I_N}{I_R + I_N}, \quad \beta = \frac{(1-s^2)}{(1+s^2)},$$

and

$$\eta = \frac{4R^2}{(1-R^2)^2}.$$

In the limit of a perfect polarizer $\gamma = \beta = 1$ and we get

$$\sin 2\Theta_F = \Delta I\left(1 + \eta\sin^2 2\Theta_F\right). \tag{A5}$$

*Also at Lincoln Laboratory, Massachusetts Institute of Technology, Lexington, MA 02173-0073.

[1] A. Gaj, R. R. Galazka, and M. Nawrocki, Solid State Commun. **25**, 193 (1978).
[2] A. E. Turner, R. L. Gunshor, and S. Datta, Appl. Opt. **22**, 3152 (1983).
[3] D. U. Bartholomew, J. K. Furdyna, and A. K. Ramdas, Phys. Rev. B **34**, 6943 (1986).
[4] P. I. Nikitin and A. I. Savchuk, Usp. Fiz. Nauk **160**, 167 (1990) [Sov. Phys. Usp. **33**, 974 (1990)].
[5] M. A. Butler, Solid State Commun. **62**, 45 (1987).
[6] A. N. Pikhtin and A. D. Yas'kov, Fiz. Tekh. Poluprovodn. **12**, 1047 (1978) [Sov. Phys. Semicond. **12**, 622 (1978)].
[7] D. T. F. Marple, J. Appl. Phys. **35**, 1241 (1964).
[8] Y. R. Lee and A. K. Ramdas, Solid State Commun. **51**, 861 (1984).
[9] J. A. van Vechten, Phys. Rev. **187**, 1007 (1969).
[10] M. Cardona, *Optical Modulation Spectroscopy of Solids*, Solid State Physics Suppl. 11 (Academic, New York, 1969).
[11] M. S. Neuberger, *Semiconducting Compounds*, Vol. 2 of *Handbook of Electronic Materials* (IFI/Plenum, New York, 1971).
[12] *Physics and Chemistry of II-VI Compounds*, edited by M. Aven and J. S. Prener (North-Holland, Amsterdam, 1967).
[13] J. Baars and F. Sorger, Solid State Commun. **10**, 875 (1972).
[14] J. Spałek, A. Lewicki, Z. Tarnawski, J. K. Furdyna, R. R. Galazka, and Z. Obuszko, Phys. Rev. B **33**, 3407 (1986).
[15] R. L. Aggarwal, S. N. Jasperson, P. Becla, and R. R. Galazka, Phys. Rev. B **32**, 5132 (1985).
[16] J. A. Gaj, R. Planel, and G. Fishman, Solid State Commun. **29**, 435 (1979).
[17] R. L. Aggarwal, S. N. Jasperson, P. Becla, and R. J. K. Furdyna, Phys. Rev. B **34**, 5894 (1986).
[18] A. Twardowski, P. Swiderski, M. von Ortenberg, and R. Pauthenet, Solid State Commun. **50**, 509 (1984).
[19] J. Ginter, J. A. Gaj, and Le Si Dang, Solid State Commun. **48**, 849 (1983).
[20] N. P. Barnes and M. S. Piltch, J. Opt. Soc. Am. **67**, 628 (1977).
[21] J. E. Harvey and W. L. Wolfe, J. Opt. Soc. Am. **65**, 1267 (1975).
[22] Northern Analytical Laboratory Inc., 23 Depot Street, Merrimack, NH 03054.

[23] Polaroid Corporation, Polarizer Division, One Upland Road, Norwood, MA 02062.
[24] PTR Optics Corp., 145 Newton St., Waltham, MA 02154.
[25] Spex Industries Inc., Box 798, Metuchen, NJ 08840.
[26] Infrared Laboratories Inc., 1808 East 17th St., Tucson, AZ 85719.
[27] Y. R. Lee, A. K. Ramdas, and R. L. Aggarwal, in *Proceedings of the 18th International Conference on the Physics of Semiconductors, Stockholm, Sweden, 1986*, edited by Olof Engström (World Scientific, Singapore, 1987).
[28] M. Cardona and D. L. Greenaway, Phys. Rev. **131**, 98 (1963).
[29] H. J. Jiménez-González, Ph.D. thesis, Massachusetts Institute of Technology, Cambridge, MA (1992).